JAST, Vol. 2, No. 1, pp 37–44
◯ Iranian Aerospace Society, month 2005

JAST
Journal of Aerospace Science and Technology

RESEARCH NOTE

A Two-Step Modification toward Implementing Compressible Source Terms in Low Compressible Flows

Masoud Darbandi[1], Seyed Farid Hosseinizadeh[2]

There is a general challenge in CFD research work either to impelement density variation in incompressible algorithms or to solve constant-density fields using compressible algorithms. A desirable extension is the one which requires a minimum number of modifications and exhibits maximum performance. In this work, an easy two-step modification scheme is introduced in order to include density variation in a specific incompressible algorithm. The modifications result in new compressible source terms in the formulations which their behaviors are studied through the solution procedure.

INTRODUCTION

As is known, incompressible methods are normally incapable of implementing the density variation in their algorithms [1]. On the other hand, compressible algorithms are widely developed for solving flow fields with high density variation [2]. The compressible methods are not basically recommended for studying low density-variation conditions [3]. Contrary to the compressible algorithms which benefit the advantages of density-based procedures, incompressible flow solvers mostly choose pressure-based procedure to solve the flow fields with invariant density. Scholars on both sides have long tried to employ suitable features or techniques in order to extend the capabilities of their algorithms for solving low density variation fields [4,5]. Generally, pressure-based methods have been more successful in solving low density variation fields. Using either pressure-based or density-based algorithms, the main objective of the algorithm developers has been to achieve the highest capabilities while implementing the least modifications in the primitive formulation. One such attempt is to take the advantages of an analogy between compressible and incompressible formulations [6]. This analogy is used to extend an arbitrary pressure-based method to take into account density variation in its primitive algorithm using minimum modifications. The analogy has been used for extending incompressible SIMPLE-based algorithms as well [7]. It is shown that the extension generally needs two modifications with respect to the primitive incompressible algorithms. The modifications can be counted as, firstly, including the compressible part of the Navier-Stokes equations into the incompressible formulations and, secondly, updating the variable density field at the end of each iteration.

One major application of low density-variation field is to solve the flow fields with heat transfer. In such flow fields, the density variation can be low or high depending on the temperature gradient between the highest and lowest temperature zones in the domain. A literature survey shows that there has been a lot of research in solving low density variation fields and few activities in solving high density variation fields. The investigators mostly employ pressure-based algorithm to solve both flow fields numerically. As is known, the buoyancy driven flow is known as a case of either low or high compressible flow fields. There are numerous applications in industry where the buoyancy performs the key role in the processes. Buoyancy driven flows are also suitable for testing compressible algorithms intend to solve low density variation fields. Choi and Merkle [8] solved the low Mach number regimes using a density-based algorithm and implementing artificial compressibility. Chenoweth and Paolucci [9] presented the results for the free convection in square cavity

1. *Associate Professor, Department of Aerospace Engineering, Sharif University of Technology, P.O. Box 11365-8639, darbandi@sharif.edu*
2. *PhD candidate, Department of Aerospace Engineering, Sharif University of Technology, hosseinizadeh@mehr.sharif.edu.*

using a pressure-based algorithm. They treated the flow as a compressible one and did not implement the classical Boussinesq approximation. Their results are very similar to those obtained from incompressible algorithms. Ismail and Scalon [10] obtained reliable results for incompressible regime using a pressure-based finite-volume-based finite-element method. Yu, et al. [11] used a least square finite element method and obtained results for compressible natural convection. Their results are different from those of incompressible algorithm.

As was mentioned, Darbandi and Hosseinizadeh [7] developed a new analogy for solving compressible flow using SIMPLE incompressible algorithm. Using this analogy, a basic incompressible numerical algorithm (SIMPLE) was generalized to solve compressible flows. However, this reference does not include the energy equation in the extension, and mainly concentrates on isothermal flows. In this paper, the analogy is suitably extended for treating low density-variation flow fields with and without heat transfer. To validate the extended formulation, the natural convection in a square cavity is selected as our test case. De Vahl Davis [12] has provided benchmark solution to this problem. His results are used to validate the current extended algorithm. In this work, the role of compressible source terms in incompressible formulations is widely investigated.

DOMAIN DISCRETIZATION

A two-dimensional solution domain is divided into a number of control volumes. The control volumes are distributed based on a staggered grid arrangement [13]. In this work, capital letter subscripts of I and J are used to enumerate the main grid lines which pass nodal points in x and y directions, respectively, and lower case subscripts of i and j are used to enumerate the grid lines which pass cell faces in the x and y-directions, respectively.

GOVERNING EQUATIONS

The two-dimensional Navier-Stokes equations in conservative forms are given by

$$\frac{\partial F}{\partial x}+\frac{\partial G}{\partial y}=\frac{\partial R}{\partial x}+\frac{\partial T}{\partial y}+B \tag{1}$$

where F, G, R, T and B are given by

$$F=(\rho u,\rho u^2+p,\rho uv\,,\,\rho uh) \tag{2}$$

$$G=(\rho v,\rho uv,\rho v^2+p\,,\,\rho vh) \tag{3}$$

$$R=(0,\tau_{xx},\tau_{xy}\,,\,\sigma_x) \tag{4}$$

$$T=(0,\tau_{yx},\tau_{yy}\,,\,\sigma_y) \tag{5}$$

$$B=(0,0\,,\,\rho_\circ g\beta(T_i-T_0),0) \tag{6}$$

The components of stress tensor, τ, are defined as

$$\tau_{xx}=2\mu\frac{\partial u}{\partial x}-\left\{\frac{2}{3}\mu(\frac{\partial u}{\partial x}+\frac{\partial v}{\partial y})\right\} \tag{7}$$

$$\tau_{yy}=2\mu\frac{\partial v}{\partial y}-\left\{\frac{2}{3}\mu(\frac{\partial u}{\partial x}+\frac{\partial v}{\partial y})\right\} \tag{8}$$

$$\tau_{xy}=\tau_{yx}=\mu(\frac{\partial u}{\partial y}+\frac{\partial v}{\partial x}) \tag{9}$$

$$\sigma_x=u\tau_{xx}+v\tau_{xy}+k\frac{\partial T}{\partial x} \tag{10}$$

$$\sigma_y=u\tau_{yx}+v\tau_{yy}+k\frac{\partial T}{\partial y} \tag{11}$$

In the above equations, T_0 is a reference temperature, ρ_0 is a reference density, β is the thermal expansion coefficient, k is the thermal conduction coefficient and g is the gravitational acceleration. The terms inside braces $\{\}$ vanish in the incompressible limit. The equation of state normally is the desired equation to calculate the density in compressible flow algorithm. If the fluid is assumed to be a calorically perfect gas, it yields

$$P=\rho RT \tag{12}$$

COMPUTATIONAL MODELING

In order to achieve a dual purpose unified algorithm, the integration of a suitable re-arrangement of the governing equations over control surface S of an arbitrary control volume in the solution domain is presented by

$$\int_S\left[F\vec{i}+G\vec{j}\right]\cdot\overrightarrow{dS}=0 \tag{13}$$

$$\int_S\left[(u)F\vec{i}+(v)F\vec{j}+P\vec{i}-v\frac{\partial F}{\partial x}\vec{i}-v\frac{\partial F}{\partial y}\vec{j}\right]\cdot\vec{dS}=s^{-x} \tag{14}$$

$$\int_S\left[(u)G\vec{i}+(v)G\vec{j}+P\vec{j}-v\frac{\partial G}{\partial x}\vec{i}-v\frac{\partial G}{\partial y}\vec{j}\right]\cdot\vec{dS}=\int_V B\,dV+s^{-y} \tag{15}$$

where $\vec{dS}$ is a vector normal to control surface, V is the volume of the control volume, and kinematics viscosity is indicated by ν. The upper case F, G, and P are chosen as the dependent variables of the solution algorithm. They will be elaborated later. At this stage, one may simply specify these variables as $F=\rho u$, $G=\rho v$, and $P=p$. The s^x, s^y source terms include both the additional diffusion terms in the compressible equations, i.e., Eqs.(7)-(9), and the additional terms which are resulted after linearizing the nonlinear diffusion terms to the desired dependent

variables [6]. For example, the latter linearization for $\mu\frac{\partial u}{\partial x}$ and $\mu\frac{\partial u}{\partial y}$ terms in Eqs.(7)-(9) yields $\mu\frac{\partial u}{\partial x} = \nu\frac{\partial F}{\partial x} - \nu\, u\frac{\partial \rho}{\partial x}$ and $\mu\frac{\partial u}{\partial y} = \nu\frac{\partial F}{\partial y} - \nu\, u\frac{\partial \rho}{\partial y}$. The bar over s means it is explicitly calculated from the known values of the parameters in the previous iteration. The proper employment of such linearizations finally results in [7]:

$$s^{-x} = \int_S \frac{\nu}{3}\left[\left\{\frac{\partial F}{\partial x} - 2\frac{\partial G}{\partial y} - 4u\frac{\partial \rho}{\partial x} + 2v\frac{\partial \rho}{\partial y}\right\}\vec{i} + 3\left\{\frac{\partial G}{\partial x} - v\frac{\partial \rho}{\partial x} - u\frac{\partial \rho}{\partial y}\right\}\vec{j}\right]\cdot d\vec{S} \quad (16)$$

$$s^{-y} = \int_S \frac{\nu}{3}\left[\left\{\frac{\partial G}{\partial y} - 2\frac{\partial F}{\partial x} + 2u\frac{\partial \rho}{\partial x} - 4v\frac{\partial \rho}{\partial y}\right\}\vec{j} + 3\left\{\frac{\partial F}{\partial y} - u\frac{\partial \rho}{\partial y} - v\frac{\partial \rho}{\partial y}\right\}\vec{i}\right]\cdot d\vec{S} \quad (17)$$

An appropriate treatment of Eqs. (14)-(15) results in two sets of algebraic equations which can be separately solved to estimate the approximate value of F^* and G^* [7]. They are derived from:

$$a_{i,J}F^*_{i,J} = \sum a_{nb}F^*_{nb} + (P^*_{I-1,J} - P^*_{I,J})A_{i,J} + b_{i,J} + s^{-x}_{i,J} \quad (18)$$

$$a_{I,j}G^*_{i,J} = \sum a_{nb}G^*_{nb} + (P^*_{I,J-1} - P^*_{I,J})A_{I,j} + b_{I,j} + s^{-y}_{I,j} \quad (19)$$

where $A_{i,J}$ and $A_{I,j}$ are the cell face areas at east (or west) and south (or north) of the u-control volume, respectively. In addition, $b_{i,J}$ and $b_{I,j}$ indicate the additional source terms in the x and y-momentum equations, respectively. The two additional source terms of $s^{-y}_{I,j}$ and $s^{-x}_{i,J}$ play no role in incompressible equations because their values are absolutely zero. Indeed, the values of the coefficients $a_{I,j}, a_{i,J}, b_{I,j}, b_{i,J}$ and a_{nb} are determined after a proper choice of a convection-diffusion model [8]. In the current work, we have employed the hybrid method.

If a pressure field, say p^*, is guessed and substituted in Eqs. (18)-(19), the two system of algebraic equations can be solved for F^* and G^*. In fact, this strategy is a trial and error tactic which is entirely analogous to an algorithm named SIMPLE [9]. SIMPLE converts the continuity equation to a pressure correction equation. This equation provides a tool to estimate the pressure correction field p' at all nodal grid points. The prime indicates the required correction to correct the star. The pressure correction magnitude is used to correct the preceding approximate solutions as:

$$P = P^* + P' \quad (20)$$

$$F_{i,J} = F^*_{i,J} + d_{i,J}(P'_{I-1,J} - P'_{I,J}) \quad (21)$$

$$G_{I,j} = G^*_{I,j} + d_{I,j}(P'_{I,J-1} - P'_{I,J}) \quad (22)$$

where $d_{i,J} = A_{i,J}/a_{i,J}$ and $d_{I,j} = A_{I,j}/a_{I,j}$. The rest of SIMPLE procedure is to solve the other discretized transport equations and to update the secondary dependent variables such as density. By this stage, the residuals are checked and if they are not low enough, the procedure is repeated for another iteration.

Although SIMPLE was originally developed for solving incompressible flow, the current algorithm enables it to consider density variation. As was explained earlier, the current ability is obtained with minimum modifications. The bases for such modification were first introduced by Reference [6]. It uses an analogy between incompressible and compressible governing equations in order to enable incompressible algorithms to solve compressible flow. The primary point in this extension is the choice of dependent variables, which result in a unique role for dependent variables in both compressible and incompressible formulations. A meaningful identification for the chosen dependent variables can be interpreted by

$$\{F, G, P\} = \begin{cases} \{u, v, p/\rho_0\} & \text{incomp.} \\ \{\rho u, \rho v, p\} & \text{comp.} \end{cases} \quad (23)$$

The p/ρ_0 division only multiplies the magnitude of the real pressure field by a constant factor of $1/\rho_0$.

By the end of this section, we should be able to classify the presented modifications in two simple steps. Step one is to add s^x and s^y to the x- and y-momentum equations as compressible source terms. They vanish in incompressible limit. Step two is to consider density variation in the algorithm. This can be achieved by including a switch in the algorithm. It updates density at the end of each iteration as:

$$\rho = \begin{cases} \rho_0 & \text{incomp.} \\ p/RT & \text{comp.} \end{cases} \quad (24)$$

The compressible equation of state is valid for a calorically perfect gas. Since the nature of flow is elliptic in low density variation fields, we do not need including a parabolic nature in Eq.(24).

RESULTS AND DISCUSSION

The extended formulations and the developed algorithm are firstly tested in a square cavity where the inside flow is driven by the upper wall/lid movement. The cavity has unit dimensions. The lid velocity is unit for incompressible case; however, the velocity depends on both Reynolds and Mach numbers in compressible flow case. The lid velocity is used to non-dimensionalize the flow field velocity components. A mesh distribution of 81×81 is fine enough to achieve the purposes in this study. However, Reference [7] performs mesh-independent study for a similar formulation in the cavity problem. The cavity is tested at Reynolds

of 1000 and three Mach numbers of 0.3, 0.6, and 0.9 as well as in the incompressible flow case.

Figures 1 and 2 present the cavity centerline velocity distributions. The U and V velocity distributions are plotted along vertical and horizontal centerlines, respectively. There are many benchmark works which the current results can be validated upon, e.g., Reference [14]. However, we do not intend to evaluate the accuracy of the current algorithm. As discussed in the preceding section, it is pure SIMPLE procedure whose performance is well-known for the CFD workers. Its accuracy remarkably depends on the method of flux approximation at control surfaces. Using a low-order hybrid approximation in this work enforces the use of finer grid for a better achievement. In the current attempt, we are to illustrate the performance of a single computational algorithm used as either a compressible or incompressible flow solver to treat low density variation fields. As is observed, irrespective of the validity of solutions, both incompressible and compressible solutions perform almost identical velocity profiles using different flow Mach numbers. Since there is a rapid drop in the velocity magnitude close to the upper lid, there is also a sharp drop in Mach number and density variation [6]. This is why all four profiles exhibit similar behaviors in Figs 1 and 2.

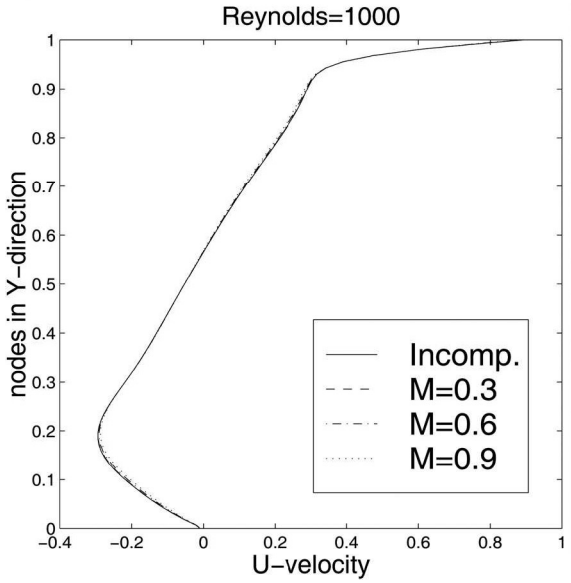

Figure 1. U velocity distribution at vertical centerline.

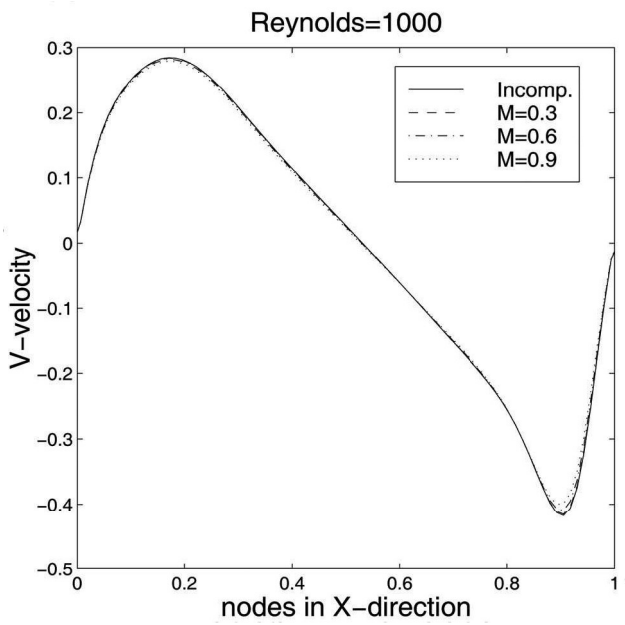

Figure 2. V velocity distribution at horizontal centerline.

As was emphasized in the Computational Modeling section, Eqs.(8)–(9) play important roles in considering density variation in the current formulations. Therefore, it is worth investigating the source term magnitude during the solution procedure. Figures 3 and 4 illustrate the maximum magnitude of the absolute value of s^x and s^y source terms VS. iteration number N. In these figures, the source terms have been nondimensionalized with ρu^2 (using unit values of 1kg/m^3 and 1 m/s). Figures show that the maximum magnitudes increase as the flow Mach number increases. These plots are well consistent with the physical behavior of the compressible source terms in the current formulations. In other words, a lower Mach number causes less density variation. For Mach numbers less than 0.3, both terms vanish. Although iteration procedure ends around N=800, the plots are restricted to N=100 because the maximum value of these source terms rapidly converge to their final

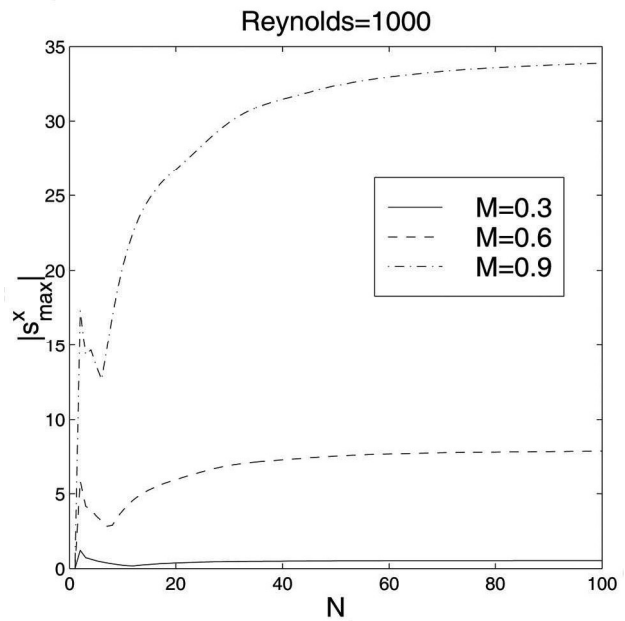

Figure 3. Maximum value of the compressible source term in x-momentum.

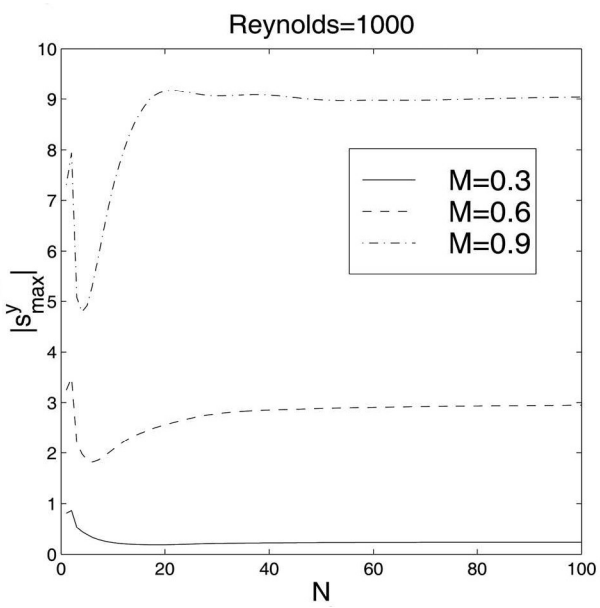

Figure 4. Maximum value of the compressible source term in y-momentum.

magnitudes. This restriction also helps to magnify the variation through early iterations.

The second test problem is the natural convection in a square cavity. The top and bottom walls of the cavity are insulated and the sidewalls are maintained at constant but different high t_h and low t_c temperatures. The fluid is assumed to be air and its properties are calculated at $t_0 = 20°C$. The Prandtle number is 0.71 and $t_h - t_c = 10°$C. The dimensions are normalized with H. The results are presented for two different Rayleigh numbers of 10^5 and 10^6. To obtain the mesh independence results, we use a 200×200 grid distribution for Rayleigh number of 10^5 and 300×300 grid distribution for Rayleigh number of 10^6. The preliminary investigation showed that these grid resolutions would suffice to obtain mesh independent solutions.

In order to present a fair evaluation of the current results, Table 1 provides sample detailed comparisons between the current results and benchmark solutions. The comparison is presented for both maximum velocity components on the centrelines of the cavity and the Nusselt number magnitudes. The results are compared with those of other reliable works [10,12,15] of which the results of Reference [12] are known as benchmark solutions. The mean heat transfer through the convecting cavity is represented by the mean Nusselt number of the domain. This number is also calculated and tabulated in Table 1 and compared with the results of the benchmark references. The present results compare favorably with the benchmark results. All the results show less than 0.72% difference at $\mathrm{Ra} = 10^5$ and 1.76% at $\mathrm{Ra} = 10^6$. As is seen, the present heat transfer results are in excellent agreement with the benchmark results.

Figures 5 and 6 present the streamlines in the convecting cavity at $\mathrm{Ra} = 10^5$ and 10^6. These streamlines have been compared with those presented by the other benchmark workers such as Reference [12,15]. There are good qualitative agreements between them. As is seen, there are two opposite vorticities in the domain at $\mathrm{Ra} = 10^5$ whereas they are broken into three smaller vorticities at higher Rayleigh numbers of $\mathrm{Ra} = 10^6$.

Similar to the cavity case, this test problem is also investigated for illustrating the behavior of the

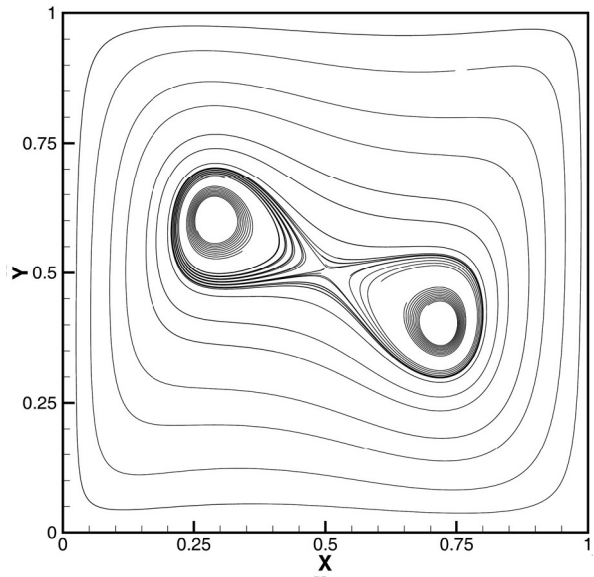

Figure 5. Streamlines in the convecting cavity at $\mathrm{Ra} = 10^5$.

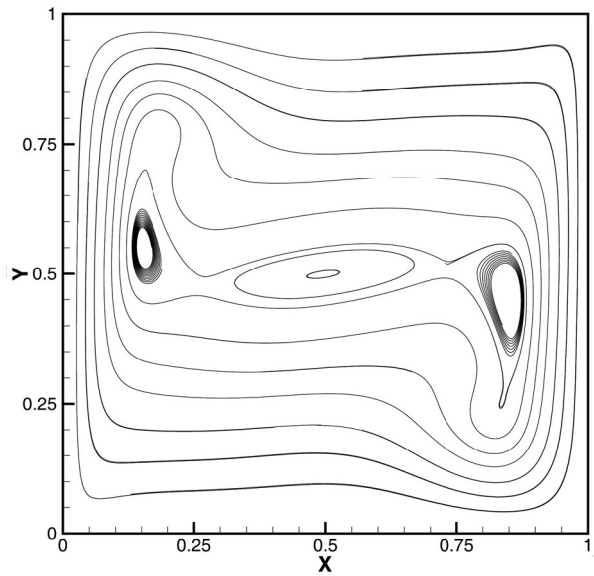

Figure 6. Streamlines in the convecting cavity at $\mathrm{Ra} = 10^6$.

Table 1. A qualitative comparison of the current solutions with those of the other works and the amount of difference.

Ra = 1E5	U_{max} (diff%)	V_{max} (diff%)	Nu_{max} (diff%)	Nu_{avg} (diff%)
Benchmark [12]	34.730	68.590	7.717	4.519
Ismail/Scalon [10]	33.421(3.77)	70.440(2.70)	7.812 (1.23)	4.651 (2.92)
Darbandi/Schneider [15]	33.40 (3.83)	70.3 (2.49)		4.562 (0.952)
This study	34.980(0.72)	68.581(0.013)	7.739 (0.29)	4.529 (0.22)
Ra = 1E6				
Benchmark [12]	64.63	219.36	17.925	8.800
Ismail/Scalon [10]	57.22(11.47)	220.48(0.51)	15.601 (12.97)	8.934 (1.52)
Darbandi/Schneider [15]	64.94(0.48)	222.2(1.295)		8.797 (0.034)
This study	65.09(0.60)	220.89(0.69)	17.610 (1.76)	8.853 (0.60)

source terms in the momentum equations. Similar to Figs. 3-4, Figures 7 and 8 depict the behavior of the maximum magnitudes of the source terms in the convecting cavity. The results indicate that the maximums vanish with the progress in the iterations. Comparing with Figs. 3-4, the global behavior is very similar to the behavior observed at low Mach number. Indeed, this is because the Mach number in the convecting cavity is dramatically low at such Rayleigh numbers and consistent with the behavior observed in Figs. 3-4 at M=0.3. However, contrary to the preceding results, the current behavior is highly oscillatory. A lower Rayleigh number indicates a lower Mach number and, consequently, a lower maximum magnitude of the source term. Of course, at higher Rayleigh numbers, the compressibility effect is important and the Buossinesq assumption cannot be valid anymore.

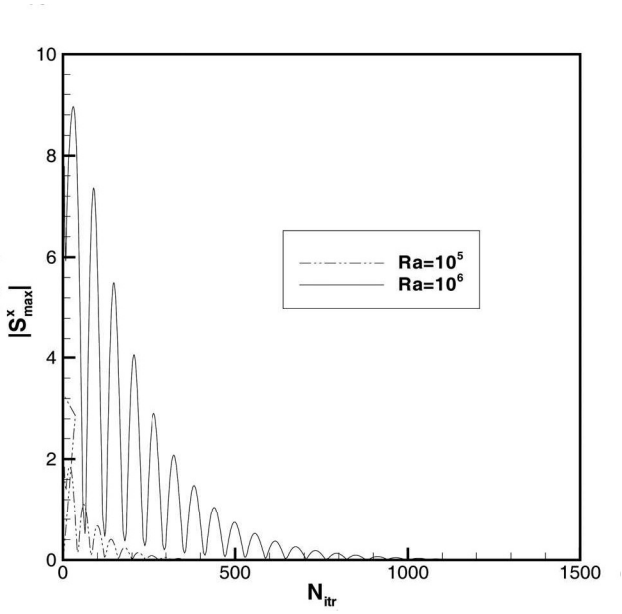

Figure 7. Maximum magnitude of s^x in the convecting cavity.

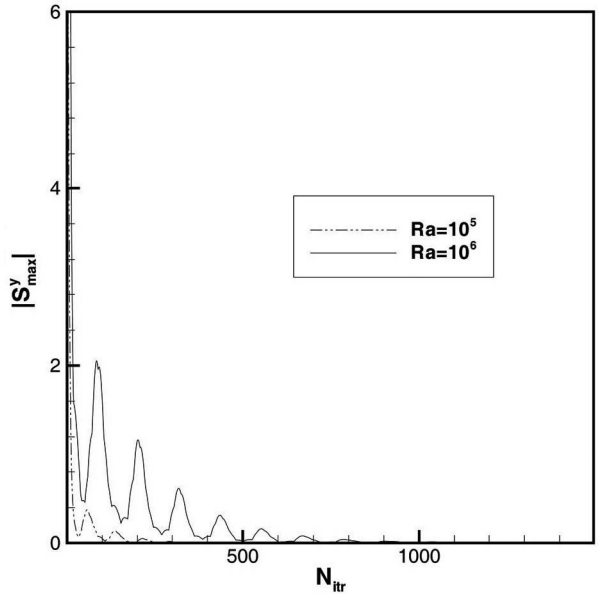

Figure 8. Maximum magnitude of s^y in the convecting cavity.

The third test case is the flow inside a channel at a Reynolds number of 20. The channel length is five times its height. The grid resolution is 300×60, which is fine enough to result in reliable accuracy. The velocity at the inlet section is a unit flat profile. The flow inside the channel passes through the developing zone and is fully developed at the exit. The problem is tested at three different Mach numbers of 0.1, 0.3, and 0.5. Reference [16] provides the details of flow through a channel at different Reynolds numbers. The reference shows that contrary to the flow variables which are remarkably mesh dependent close to the channel boundaries, the centerline magnitudes are less mesh dependent and reliable solutions can be achieved using

coarse grid distributions. Here, we intend to study the compressibility source terms in the incompressible formulations. Figure 9 shows the pressure distribution along the centerline of the channel at the three Mach numbers. As is observed, a higher pressure difference is required in higher compressible flow cases. Irrespective of the Mach number, the pressure at the exit is fixed. It is because we implement similar boundary conditions at the outlet section in all cases.

Figures 10 and 11 present the behavior of the maximum magnitudes of the source terms in the channel. The behavior is very similar to those observed in the first test case. The figures show that the weight of compressibility at higher Mach number is dominant enough to increase the number of iterations drastically.

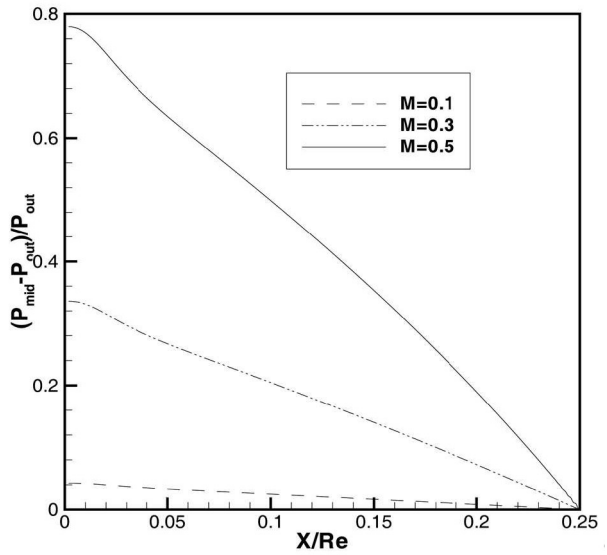

Figure 9. Pressure distribution along the centreline of channel, Re = 20.

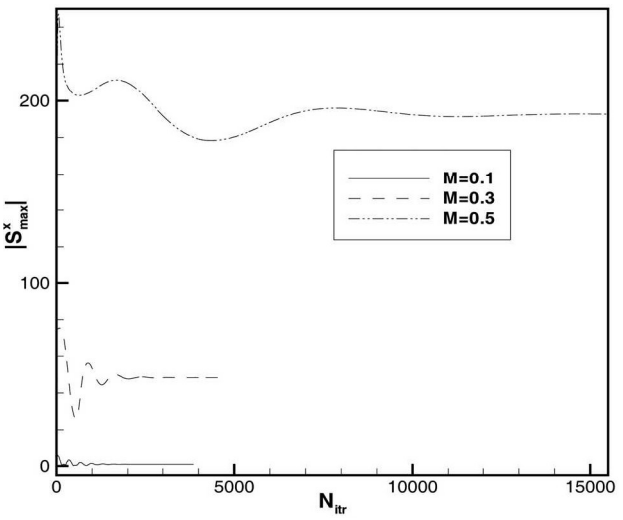

Figure 10. Maximum magnitude of s^x in the channel.

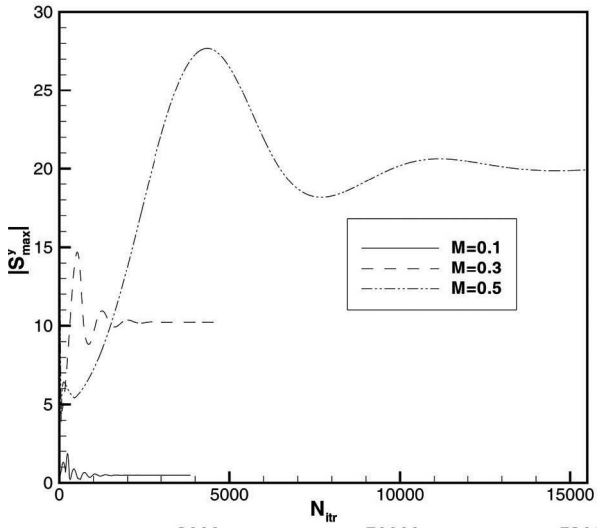

Figure 11. Maximum magnitude of s^y in the channel.

As are observed, the magnitudes of source terms are not much lower at higher Mach numbers in this test case.

CONCLUSION

Using a pure incompressible algorithm incorporated the compressible source terms, a new two-step procedure was developed to take into account the density variation in low compressible flow fields. The algorithm was tested by studying three types of low density variation regimes. The test cases were chosen in a manner which permitted to consider density variation as a result of either pressure variation or temperature variation as well as their combined variations. Then, the role of compressible source terms in the incompressible formulation was deeply investigated. Obviously, the compressibility effect becomes dominant at higher Mach numbers. Despite the higher compressibility effect at higher Mach numbers, the current developed compressible formulation (which is solved in a pure incompressible algorithm) is not deteriorated, and provides solutions with suitable accuracy comparable to those of benchmark solutions. The accuracy increases with grid refinement due to the use of a first-order hybrid scheme to approximate the fluxes at cell faces. The developed algorithm showed excellent performance in all test cases. The two-step procedure can be easily implemented in any SIMPLE-based incompressible algorithm to solve the low density variation regimes. This type of regime has numerous applications in the heat transfer study where the Buossinesq assumption fails to provide suitable approximation for the influence of the buoyant force.

ACKNOWLEDGEMENT

The authors wish to thank the Research Center at Sharif University of Technology for funding the present study.

REFERENCES

1. Kobayashi M. H., and Pereira J. C. F., "Calculation of Incompressible Laminar Flows on a Nonstaggered, Nonorthogonal Grid", *Numerical Heat Transfer*, Part B, **19**, PP 243-262(1991).
2. Hassan O., Morgan K., and Peraire J., "An Implicit/Explicit Scheme for Compressible Viscous High Speed Flows", *Computer Methods in Applied Mechanics and Engineering*, **76**, PP 245-258(1989).
3. Volpe G., "Performance of Compressible Flow Codes at Low Mach Numbers", *AIAA Journal*, **31**, PP 49-56(1993).
4. Bressloff N. W., "A Parallel Pressure Implicit Splitting of Operators Algorithm Applied to Flows at all Speeds", *International Journal of Numerical Methods in Fluids*, **36**, PP 497-518(2001).
5. Mary I., Sagaut P., and Deville M., "Algorithm for Low Mach Number Unsteady Flows", *Computers and Fluids*, **29**, PP 119-147(2000).
6. Darbandi M., and Schneider G. E., "Analogy-Based Method for Solving Compressible and Incompressible Flows", *AIAA Journal of Thermophysics and Heat Transfer*, **12**, PP 239-247(1998).
7. Darbandi, M., and Hosseinizadeh S.F., "General Pressure-Correction Strategy to Include Density Variation in Incompressible Algorithms", *AIAA Journal of Thermophysics and Heat Transfer*, **17(3)**, PP 372-380(2003).
8. Choi, Y.H., and Merkle, C.L., "Computation of Low Speed Flow with Heat Addition", *AIAA Journal*, **25**, PP 831-838(1987).
9. Chenoweth, D.R., and Paolucci, S., "Natural Convection in an Enclosed Vertical Air Layer with Large Horizontal Temperature Differences", *Journal of Fluid Mechanics*, **169**, PP 173-210(1986).
10. Ismail, K. A. R., and Scalon, V. L., "A Finite Element Free Convection Model for the Side Wall Heated Cavity", *International Journal of Heat and Mass Transfer*, **43**, PP 1373-1389(2000).
11. Yu, S.T., Jiang, B.N., Wu, J., and Liu, N.S., "A Div-Curl-Grad Formulation for Compressible Buoyant Flows Solved by the Least-Squares Finite Element Method", *Computer Methods in Applied Mechanics and Engineering*, **137**, PP 59-88(1996).
12. De Vahl Davis, G., "Natural Convection of Air in Square Cavity: A Benchmark Solution", *International Journal of Numerical Methods in Fluids*, **3(10)**, PP 249-264(1983).
13. Versteeg, H. K., and Malalasekera W., *An Introduction to Computational Fluid Dynamics; The Finite Volume Method*, Addison Wesley Longman Limited, (1995).
14. Botella, O., and Peyret, R., "Benchmark Spectral Results on the Lid-Driven Cavity Flow", *Computers & Fluids*, **27(4)**, PP 421-433(1998).
15. Darbandi, M., and Schneider, G.E., "Thermobuoyancy Treatment for Electronic Packaging Using an Improved Advection Scheme", *ASME Journal of Electronic Packaging*, **125**, PP 244-250(2003).
16. Darbandi, M., and Hosseinizadeh, S.F., "Remarks on Numerical Prediction of Wall Shear Stress in Entry Flow Problems", *Communications in Numerical Methods in Engineering*, **20(6)**, PP 619-625(2004).